J Electr Eng Technol.2018; 13(5): 2134-2143
http://doi.org/10.5370/JEET.2018.13.5.2134

ISSN(Print) 1975-0102
ISSN(Online) 2093-7423

Fault Diagnosis of Transformer Based on Self-powered RFID Sensor Tag and Improved HHT

Tao Wang*, Yigang He†,, Bing Li* and Tiancheng Shi***

Abstract – This work introduces a fault diagnosis method for transformer based on self-powered radio frequency identification (RFID) sensor tag and improved Hilbert-Huang transform (HHT). Consisted by RFID tag chip, power management circuit, MCU and accelerometer, the developed RFID sensor tag is used to acquire and wirelessly transmit the vibration signal. A customized power management including solar panel, low dropout (LDO) voltage regulator, supercapacitor and corresponding charging circuit is presented to guarantee constant DC power for the sensor tag. An improved band restricted empirical mode decomposition (BREMD) which is optimized by quantum-behaved particle swarm optimization (QPSO) algorithm is proposed to deal with the raw vibration signal. Compared with traditional methods, this improved BREMD method shows great superiority in reducing mode aliasing. Then, a promising fault diagnosis approach on the basis of Hilbert marginal spectrum variations is brought up. The measured results show that the presented power management circuit can generate 2.5V DC voltage for the rest of the sensor tag. The developed sensor tag can achieve a reliable communication distance of 17.8m in the test environment. Furthermore, the measurement results indicate the promising performance of fault diagnosis for transformer.

Keywords: Transformer fault diagnosis, Self-powered, RFID, Improved BREMD.

1. Introduction

The power transformer plays a dominant role in the power grid, and its operation state is of great significance to the reliability of the power grid. Electrical, mechanical and thermal failures are considered as three main failure categories of transformer [1-3]. The mechanical failures resulted from windings or core leads to the most serious results, which would cause considerable economic loss. Fault diagnosis is a process employed to determine the operation conditions of power transformer, which can detect the failure in early stage. The conventional fault diagnosis methods for transformer such as short circuit reactance [4], dissolved gas analysis (DGA) [5] and frequency response analysis (FRA) [6] have been widely employed. Nevertheless, the noninvasive and cost-efficient methods are still actively demanded.

In the past few years, several vibration-based fault diagnosis methods have been proposed owing to the merits of nondestructive and live-line measurement. Moreover, the vibration signal is closely related to the structure change of transformer, which further increases its popularity [7-9]. Hong *et al*. [10] deduce a health indicator that can determine the condition of transformer. Garcia *et al*. [11] establish a tank vibration model by using the fundamental frequency of windings, which can distinguish the healthy and abnormal transformer. However, for transformer in service, there are varieties of background noises and harmonic components jamming in the windings and core vibration, which makes it difficult to effectively extract the health indicator. What's more, the nonlinear and non-stationary features of the vibration signals further increase the difficulty of health indicator extraction. To date, the time-frequency method has raises great interests since it can pervasively and accurately revel the characteristics of the vibration signals [12, 13]. Hilbert-Huang Transform (HHT) that includes empirical mode decomposition (EMD) and Hilbert spectrum analysis has been widely used in analyzing nonstationary and nonlinear signals [14-16]. However, the traditional EMD shows serious aliasing phenomenon and unable to describe the multiple-frequency signal effectively. The ensemble EMD (EEMD) [17] and band restricted EMD (BREMD) [18] are two improved methods to solve the abovementioned problems. But there are still limitations such as the blindness of noise choice and the error in masking signal calculation. In [13] multiple-frequency EMD (MFEMD) is proposed, it absorbs the quintessence of conventional EMD methods and shows good performance in extracting features of non-linear and non-stationary signals, but the parameters are chosen based on practical experience, which has low stability in performance of feature extracting. Thus in this paper, quantum-behaved particle swarm optimization (QPSO)

† Corresponding Author: Dept. of Electrical Engineering and Automation, Hefei University of Technology, China. (18655136887@163.com)
* Dept. of Electrical Engineering and Automation, Hefei University of Technology, China. (libinghnu@hfut.edu.cn)
** Dept. of Electrical Engineering, Wuhan University, China.
Received: December 14, 2017; Accepted: March 27, 2018

algorithm [19] is used for parameter selection of the BREMD, which promises good performance in solving aliasing phenomenon and feature extraction.

Accurate vibration signal acquisition is the fundamental of effective fault diagnosis. Generally, vibration signals of transformer are acquired by traditional accelerometer which are fixed on the transformer tank wall, its reliability has proven to be acceptable [20, 21]. Nevertheless, the high costs for its implementation and maintenance limits it being widely employed. The past few years has witnessed the evolution of radio frequency identification (RFID) technologies, especially in industrial applications [22, 23]. Catarinucci *et al.* [24] introduces an improved RFID sensor tag by integrating the sensing functionality into the passive RFID tag and realizes remarkable size reduction, but the reliable operation distance of this RFID sensor tag range up to 4 m, which is far less than the safely accessible distance of power transformer. Danilo *et al.* [25] develops the double antenna RFID sensor tag that increases the maximum communication distance to 10m. However, this sensor tag still utilizes antenna for energy harvesting, which could be invalid when the sensor tags are undergoing situations including interference, misalignment between different sensor tag antenna and reader antenna. To further increase the communication distance and improve the operation reliability of sensor tag, this paper presents a novel self-powered RFID sensor tag which scavenges energy from surrounding environment. Appreciable energy sources could be utilized by the proposed sensor tag, solar energy is proven to be simple yet effective [26-28]. Nevertheless, the solar energy is sensitive to weather conditions (e.g. illumination intensity and temperature), so in this paper, supercapacitor is employed to guarantee the stable performances of the proposed sensor tag. Moreover, to further improve the stability of solar power supply, a customized charging circuit for the supercapacitor is developed.

This paper makes significant progress in the realization of a fault diagnosis method for transformer with merits of noninvasive, miniaturized, cost-effective and high reliability. This paper are organized as following: Section II presents the sensor tag architecture and its implementation. The theories are introduced in Section III. The corresponding measurement results and discussion are presented in Section IV. Section V draws the conclusion.

2. RFID Sensor Tag Design

2.1 Sensor tag architecture

The architecture of the developed self-powered RFID sensor tag is shown in Fig. 1. In addition to the typical identification function, this RFID sensor tag also has functionalities of energy harvesting, sensing, data storage, processing and wireless delivering. The power needed for

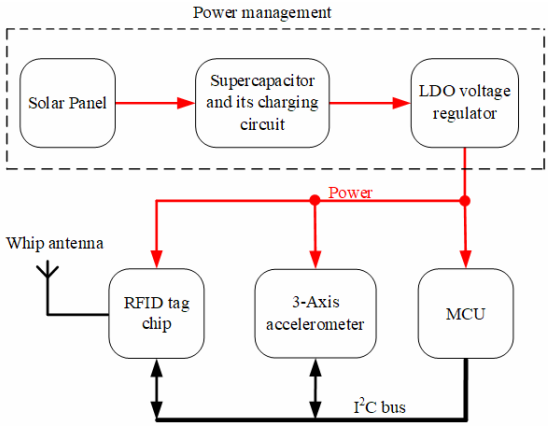

Fig. 1. Architecture of the proposed RFID sensor tag

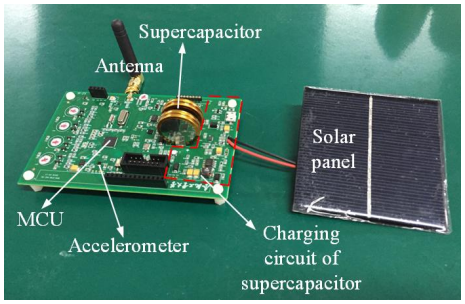

Fig. 2. Proposed RFID sensor tag

operation can be scavenged by the solar panel, and the power management circuitry is designed to increase the continuity of power supply of the solar panel. The low dropout voltage regulator (TPS780180300DRVR) is used to guarantee 2.5-V DC voltage for the sensor tag. In this work, MSP430FR5992 MCU that can provide 256 kB of Ferroelectric Random Access Memory (FRAM) is used for signal processing, the power consumption of this MCU is 118 μA/MHz in active mode. ADXL372 is a 3-axis accelerometer which is adopted for vibration signal acquisition in this design, it requires 22 μA in measurement mode (2.5V input voltage). The adopted RFID chip is a typical Monza X-8K, both the I2C interface and wireless UHF interface can access its memory. Fig. 2 is the prototype of the presented RFID sensor tag.

2.2 Power management

The power management consists of solar panel, charging circuit, supercapacitor, and voltage regulator, among which the charging circuit (shown in Fig. 3) is customized to improve the performance of solar power supply. In general, a solar energy controller based on maximum power point tracking (MPPT) should be used to achieve maximum power output. But this method would increase the costs and complexity of the sensor tag. Thus, in this paper, supercapacitor is adopted to simplify the topology structure and realize sustainable operation of the sensor tag.

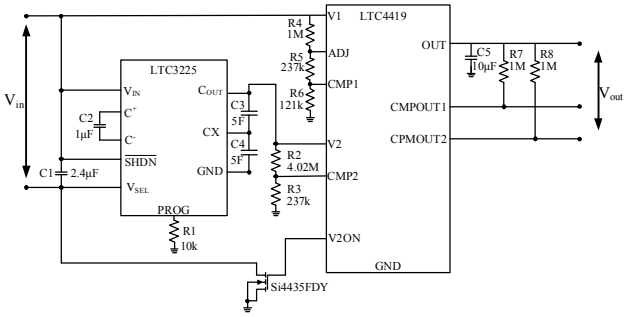

Fig. 3. The structure of charging circuit

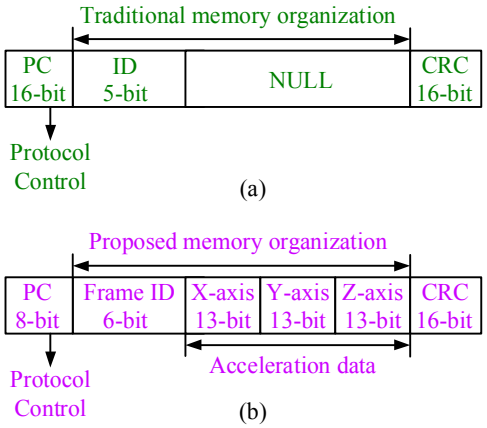

Fig. 4. Comparison of memory organization: (a) the proposed organization; (b) conventional organization

Since the solar energy cannot thought to be reliable enough, two supercapacitors (C3 and C4) in series are adopted in this paper as backup power supply. LTC3225 [29] is a supercapacitor charger that can charge the two supercapacitors to an optional output voltage (4.8V), but it cannot determine the priority of the two power supplies above. Hence, a micro-power PowerPath prioritizer (LTC4419 [30]) is employed to determine the primary power source (solar panel). During the daytime, power from the solar panel is used to charge the supercapacitor and power the sensor tag. When the output voltage of solar panel is lower than 2.8V, the supercapacitor starts to power the sensor tag. Detailed tests for power management is shown in section IV part B.

2.3 Communication strategy

An obvious merit of the sensor tag is the data measured by sensor could be stored in RFID chip memory. Fig. 4 shows the differences between the traditional memory organization and the proposed memory organization. As can be seen, the data measured by the sensor tag (Acceleration data) is sent to the memory of RFID tag chip via I^2C bus. The sensor tag can be identified by the Frame ID, which is different from each other.

The proposed RFID sensor tag can operates in both passive can self-powered mode. Within the operation range

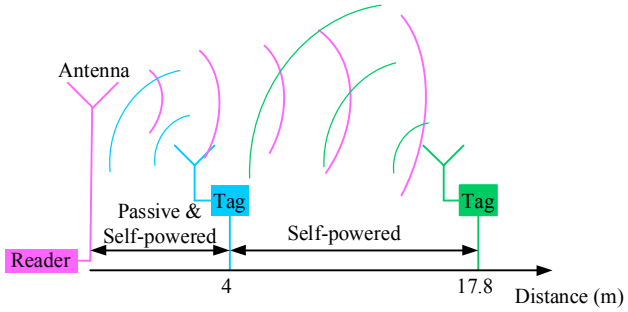

Fig. 5. Operation mode of the sensor tag under different communication distance

of 4m, both the antenna and the solar panel can harvest energy to power the sensor tag. For operation distance beyond 4m, the energy harvested by the tag antenna is not sufficient for the whole sensor tag, thus the solar panel is then to be the only power source. Limited by the size and efficiency of solar panel, the reliable operation range up to 17.8m. The whole operation modes are drawn in Fig. 5.

3. Theory

3.1 BREMD

The BREMD is a sifting process by which the IMFs can be obtained [18]. Assuming that the raw signal is $x(t)$, then it can be decomposed into:

$$x(t)=\sum_{i=1}^{n} c_i(t)+r_n(t) \tag{1}$$

where $c_i(t)$ is the i-th IMF and $r_n(t)$ is a residual. Following are the specific procedures of BREMD:

Step 1: decompose the raw signal $x(t)$ by conventional EMD to obtain the first IMF denoted IMF1.

Step 2: apply Hilbert Transform to IMF1 and the instantaneous frequency and amplitude are then obtained, the frequency of masking signal can be calculated by:

$$f_{mask}=A\frac{\sum_{i=1}^{k} a_1(i)f_1^2(i)}{\sum_{i=1}^{k} a_1(i)f_1(i)} \tag{2}$$

where A is the bandwidth coefficient, $a_1(i)$ and $f_1(i)$ represent the instantaneous amplitude and frequency of IMF1, respectively.

Step 3: construct the masking signal as:

$$m(t)=A_0\sin(2\pi f_{mask}t) \tag{3}$$

where A_0 is the amplitude coefficient decided by the average amplitude of IMF1.

Step 4: apply EMD again to a new signal $y(t)=x(t)+m(t)$

and the first IMF of $y(t)$ denoted IMF1$_s$ is then obtained. Thus, the first IMF of the raw signal denoted $c_1(t)$ can be obtained by:

$$c_1(t) = IMF1_s - m(t) \tag{4}$$

Step 5: repeating steps *1-4* until obtains all IMFs

The performance of BREMD in solving mode aliasing phenomena highly relies on the bandwidth coefficient A in equation (4), however, the selection of A is generally based on experience, so it cannot always satisfy the requirements in application. Therefore, quantum-behaved particle swarm optimization (QPSO) algorithm is adopted to optimize the selection of A.

3.2 QPSO

Inspired by quantum mechanics, the QPSO is proposed to determine the optimal solution in a search space [19]. In the QPSO algorithm, the population is seen as a swarm, the state of the each particle is considered as a potential solution in the searching space and it is depicted by a wave function instead of the position and velocity as in the particle swarm optimization (PSO) algorithm. In the search space, $X_i(t)$ is the current position of i-th particle in t-th generation. The particles update their position according to the following equation:

$$\begin{aligned} &X_i(t+1) = P(t) \pm \alpha \left| mbest - X_i(t) \right| \ln(1/u), \quad u \sim U(0,1) \\ &P(t) = \mu P_{I,i}(t) + (1-\mu) P_{G,i}(t), \quad \mu \sim U(0,1) \\ &mbest = \frac{1}{M} \sum_{i=1}^{M} P_{I,i}(t) \end{aligned} \tag{5}$$

where $P(t)$ is the local attractor of the i-th particle, α is contraction-expansion coefficient, *mbest* denotes the mean value of the best positions for all particles, u and μ are parameters that are distributed uniformly within [0,1], $P_{I,i}$(t) and $P_{G,i}$(t) are the individual best position and global best position of i-th particle in t-th generation. M is the number of particles.

To obtain the optimal performance in suppressing mode aliasing, an indicator K_M is defined as the fitness function of QPSO algorithm.

$$K_M = 1 - \frac{W_1}{\sum_{i=1}^{k} W_i} \tag{6}$$

where W_1 is the amplitude of dominant frequency components which has the higher frequency and greater amplitude in an IMF. W_1 to W_k represent the amplitudes of frequency components other than the dominant frequency. K_M is within [0, 1], and smaller K_M means better performance of suppressing mode aliasing. In this paper, when K_M <0.05, the obtained A_0 is regarded as acceptable.

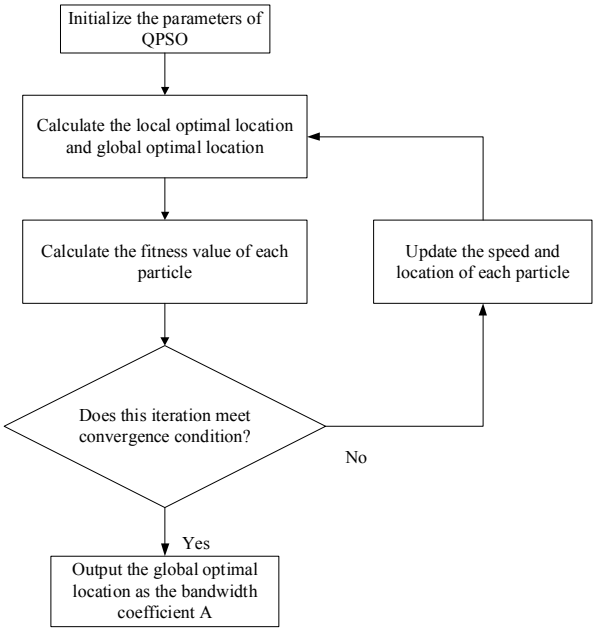

Fig. 6. Flow chart of bandwidth coefficient optimization by using QPSO

The whole procedures to find the optimal value of A are shown in Fig. 6.

3.3 Fault diagnosis

In this paper, the Hilbert marginal spectrum (HMS) which describes the total amplitude contribution of each frequency is employed to realize fault diagnosis for the transformer. As abovementioned, the raw signal is decomposed into a series of IMFs ($c_i(t)$), according to Hilbert transform, the Hilbert spectrum of each IMF is then obtained:

$$H[c_i(t)] = \frac{1}{\pi} \int \frac{c_i(\tau)}{t-\tau} d\tau \tag{7}$$

z_i(t) is defined as:

$$z_i(t) = c_i(t) + jH[c_i(t)] = a_i(t) e^{i\varphi_i(t)} \tag{8}$$

where $a_i(t)$ and $\varphi_i(t)$ are the instantaneous amplitude and phase of $c_i(t)$, respectively. They can be obtained by the following equation:

$$\begin{aligned} &a_i(t) = \sqrt{c_i^2(t) + H^2[c_i(t)]} \\ &\varphi_i(t) = \arctan \frac{H[c_i(t)]}{c_i(t)} \end{aligned} \tag{9}$$

Then, the instantaneous frequency $f_i(t)$ can be obtained:

$$f_i(t) = \frac{d\varphi_i(t)}{2\pi \cdot dt} \tag{10}$$

The HMS can calculated as follows:

$$h(f)=\int_{-\infty}^{\infty}(\mathrm{Re}\sum_{i=1}^{n}a_i(t)e^{j\int f_i(t)dt})dt \quad (11)$$

The HMS of transformer under normal condition is set as a reference, by calculating the similarity between the reference and HMS obtained from vibration signals that were acquired from transformer in service, the condition of transformer can be determined. The similarity of two HMS can be calculated as follows:

$$s_{tag,\,ref}=\frac{\sum_{i=1}^{T}\left|(tag_m(i)-\bar{tag}_m)(ref(i)-\bar{ref})\right|}{\sqrt{(\sum_{i=1}^{T}(tag_m(i)-\bar{tag}_m)^2)(\sum_{i=1}^{T}(ref(i)-\bar{ref})^2)}}\times 100\% \quad (12)$$

$$\bar{tag}_m=\frac{1}{T}\sum_{i=1}^{T}tag_m(i) \quad (13)$$

where m is the sensor tag numbers, T is the length of HMS, i is the sample number, $s_{m,n}(tag_m, ref)$ denotes the similarity. A larger value of $s_{m,n}(tag_m, ref)$ means higher similarity between the HMS of tag_m and reference. In this paper, when $s_{m,n}(tag_m, ref)$>90%, the two spectrums can be regarded as similar, and when $s_{m,n}(tag_m, ref)$ <60%, it is regarded as dissimilar. Therefore, when $s_{m,n}(tag_m, ref)$<60%, the transformer is thought to be abnormal.

4. Measurement Results

4.1 Power management

Since the solar panel performs like a current source and its output voltage keeps changing over time, the power management circuit shown in Fig. 1 is customized to improve the performance of solar panel and realize sustainable operation of proposed sensor tag. Fig. 7 shows the evolution of output voltage from solar panel, supercapacitor, and voltage regulator in a 24-hour period.

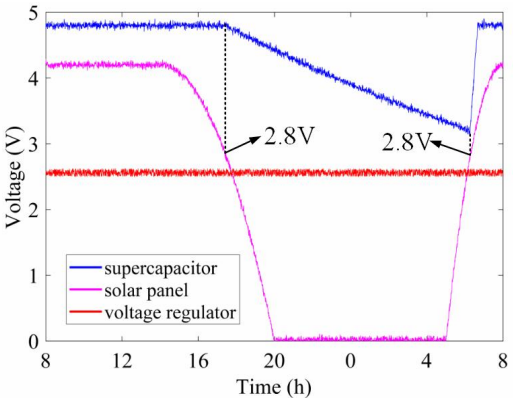

Fig. 7. Output voltage of power management

As can be seen, the voltage regulator provides stable 2.5V DC output voltage in the whole period. When the output voltage of solar panel drops below 2.8V, the input V1 (in Fig. 3) becomes invalid and the switchover to V2 occurs, and then the supercapacitor starts to work.

Since the supply voltage to the sensor tag is fixed at 2.5V, the whole power consumption of the RFID sensor tag is determined by the consumed current. Hence, the experimental setup shown in Fig. 8 is employed to measure the consumed current, the proposed sensor is powered by a DC power supply (Kikusui PMX-35A), and the consumed current is measured by a digit multimeter (Keithley 2010). The developed sensor tag is activated every 30ms by a RFID reader. As shown in Fig. 9, the current consumption of the sensor tag is 523μA during the process of acceleration sensing and RFID communication. The proposed sensor tag still has a current consumption of 4.2μA in sleep mode.

In this paper, LTC3225 which requires 2.8V DC input voltage is adopted to charge the supercapacitor. To

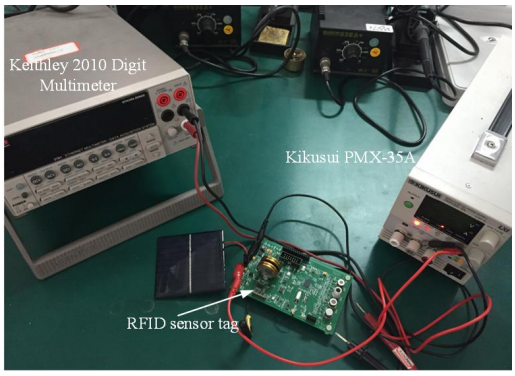

Fig. 8. Measurement setup for current consumption

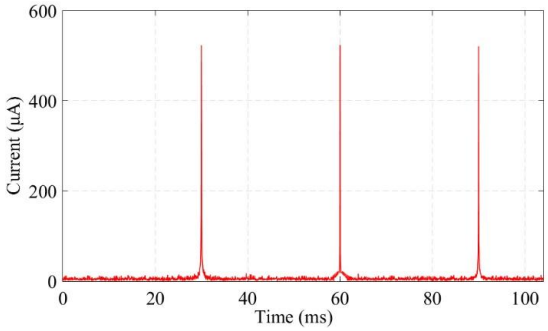

Fig. 9. Measured current consumption

Table 1. Charging time of supercapacitors

Time	Initial voltage(V)	Final voltage(V)	Charging time(s)
8:00-8:30	2.79	4.80	43
9:30-10:00	2.80	4.79	44
11:00-11:30	2.81	4.81	43.5
14:00-14:30	2.8	4.81	42
15:30-16:00	2.78	4.80	43
17:30-18:00	2.8	2.81	/

evaluate its charging ability, the charging time of supercapacitor is measured during the daytime, Table 1 shows the measurement results. As can be seen, the average charging time is 43.1s, which is deemed to be acceptable in practical applications.

4.2 Communication performance

In this paper, the operating frequency of the sensor tag is set as 915M, and a customized RFID tester (VISN-R1200) [31] is employed to test its communication performance. The distance between the tester antenna and the proposed RFID sensor tag is 1m, and the RF power of the tester is 4W. Fig. 10 illustrates the measured communication flow. As can be seen, the tester firstly sends the Select instruction to the sensor tag. After 5 Tari (1 Tari=12.5 μs), the tester sends Query instruction, and then the sensor tag responses with RN16 instruction. Next, the tester sends Acknowledgement (ACK) instruction to obtain the sensor data and corresponding ID. The REQ_RN instruction is then sent to the sensor tag to acquire the Handle reply.

The maximum operation distance is a vital parameter of the sensor tag, hence, a Gen2 RFID reader (VISN-V3) is adopted to measure it. Both the reader antenna and the proposed sensor tag are fixed in the line of sight. The distance between the reader and the sensor tag is increased in steps of 1 m, at measurement distance, 1000 reading instructions are executed to read from sensor tag. The distances where the success ratio (the ratio of successful reading numbers to total reading numbers) is higher than 80% are deemed to be reliable communication distances. Fig. 11 illustrates the measured success ratio at different distance. As seen, the success ratio exceeds 80% up to 17.8m, which exceeds the safely accessible distance of transformer.

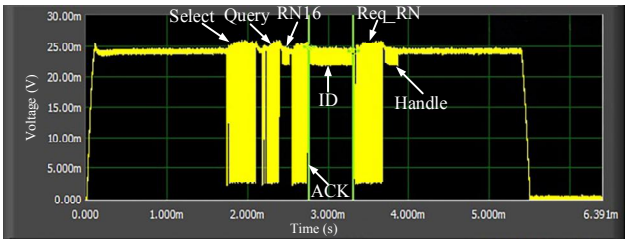

Fig. 10. Overall communication flow

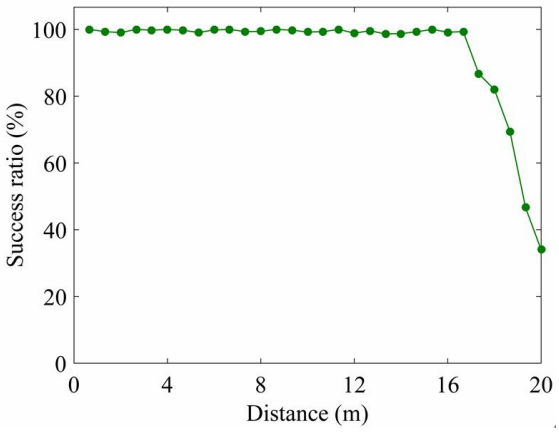

Fig. 11. Success ratio vs. distance

4.3 Fault diagnosis

The experimental object is an 110kV three-phase (represented by A, B, and C) oil-immersed transformer. Six RFID sensor tags are fixed on the transformer tank to acquire the vibration signals. Both the photograph and block diagram are shown in Fig. 12(a) and (b), respectively. The main parameters of the transformer are listed in Table 2.

The proposed sensor tags are used to measure the vibration data of a unload transformer in normal condition. Fig. 13 shows the measured waveform of the six sensor tags.

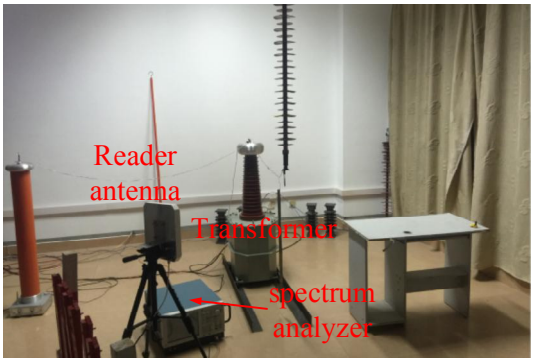

(a)

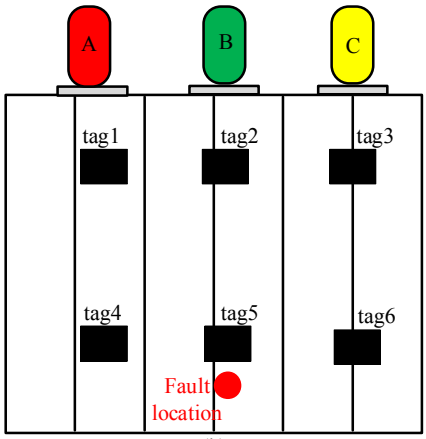

(b)

Fig. 12. Experimental setup of fault diagnosis: (a) experiment environment; (b) sensor tags' location and fault location

Table 2. PARAMETERS OF TESTING TRANSFORMER

Primary voltage (kV)	Secondary voltage (kV)	Rated power (MW)
10	3.5	10

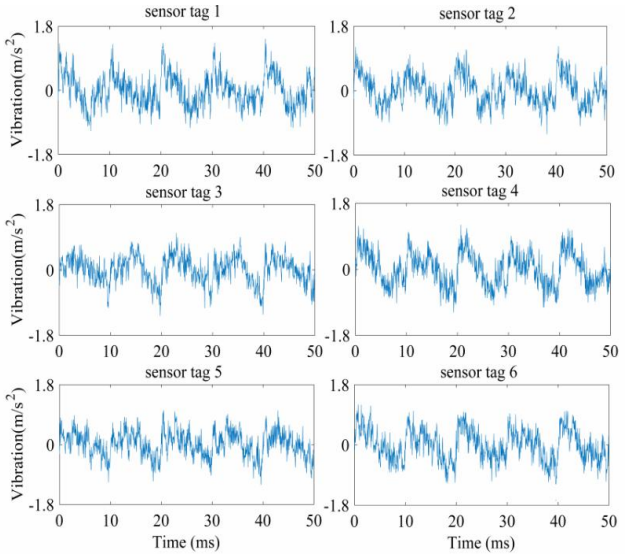

Fig. 13. Vibration signals of transformer under normal condition

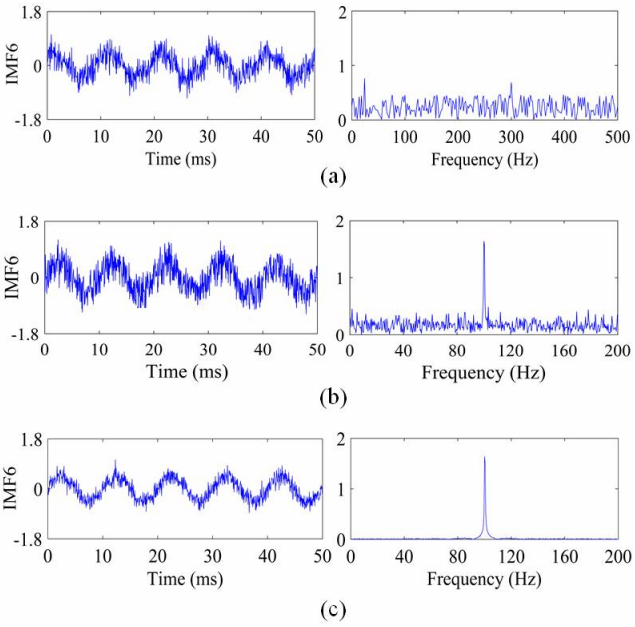

Fig. 14. IMF6 decomposed by three different methods and the corresponding FFT spectrum: (a) EMD; (b) BREMD; (c) QPSO-EMD

The vibration signals from sensor tag 1 are selected as the analysis object. Since 100Hz is the main frequency components in the whole vibration signal [10], its corresponding IMFs (IMF6) and Hilbert marginal spectrum obtained by three different methods (EMD, BREMD, and QPSO-EMD) are illustrated in Fig. 14. As seen, the results of EMD is in a mass and the characteristics are unclear; BREMD can clearly extract the Eigen-frequency, however, the aliasing phenomenon is still severe. The QPSO-EMD can effectively extract the Eigen-frequency and obtain a clearly result.

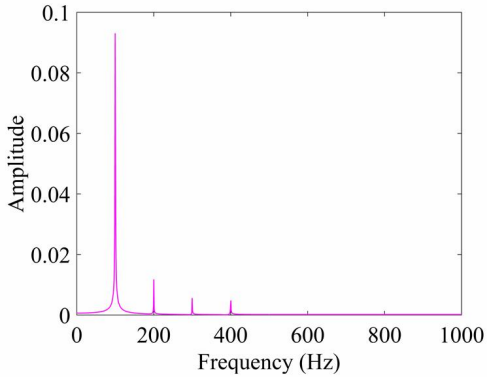

Fig. 15. Hilbert marginal spectrum of normal condition

Table 3. Similarities of Hilbert marginal spectrum

Similarity (%)	Tag1	Tag2	Tag3	Tag4	Tag5	Tag6
Tag1	100	95.1	93.6	92.8	93.9	94.1
Tag2	95.1	100	91.7	96.6	95.2	96.3
Tag3	93.6	91.7	100	93.5	92.2	95.3
Tag4	92.8	96.6	93.5	100	94.5	93.2
Tag5	93.9	95.2	92.2	94.5	100	92.9
Tag6	94.1	96.3	95.3	93.2	92.9	100

Table 4. Hilbert marginal spectrum similarities between core deformation and normal condition

Sensor tag	1	2	3	4	5	6
$S_{tag,\ ref}$ (%)	53.6	50.3	48.5	43.2	40.4	45.1

Table 5. Hilbert marginal spectrum similarities between winding deformation and normal condition

Sensor tag	1	2	3	4	5	6
$S_{tag,\ ref}$ (%)	37.3	35.3	38.7	28.2	23.4	27.1

Table 6. Hilbert marginal spectrum similarities between winding looseness and normal condition

Sensor tag	1	2	3	4	5	6
$S_{tag,\ ref}$ (%)	31.5	30.3	32.7	21.2	16.4	22.3

In Fig. 15 the Hilbert marginal spectrum of vibration signal from sensor tag 5 under normal condition is described, it is clearly that the vibration is mainly focused on 100Hz, the amplitudes of harmonic components is much smaller than the 100Hz component. In this paper, three different fault conditions (winding deformation, core deformation, winding looseness,) are employed to validate the feasibility of the proposed method.

Table 3 shows the similarities of Hilbert marginal spectrum from all the six sensor tags. It is obviously that the similarities are all greater than 90%, which means that the vibration distributions of healthy transformer are almost the same in different locations.

Three different fault conditions (core deformation, winding deformation, and winding looseness) are employed to validate the feasibility of the proposed diagnosis method, the location of the faults are shown in Fig. 12(b). Limited

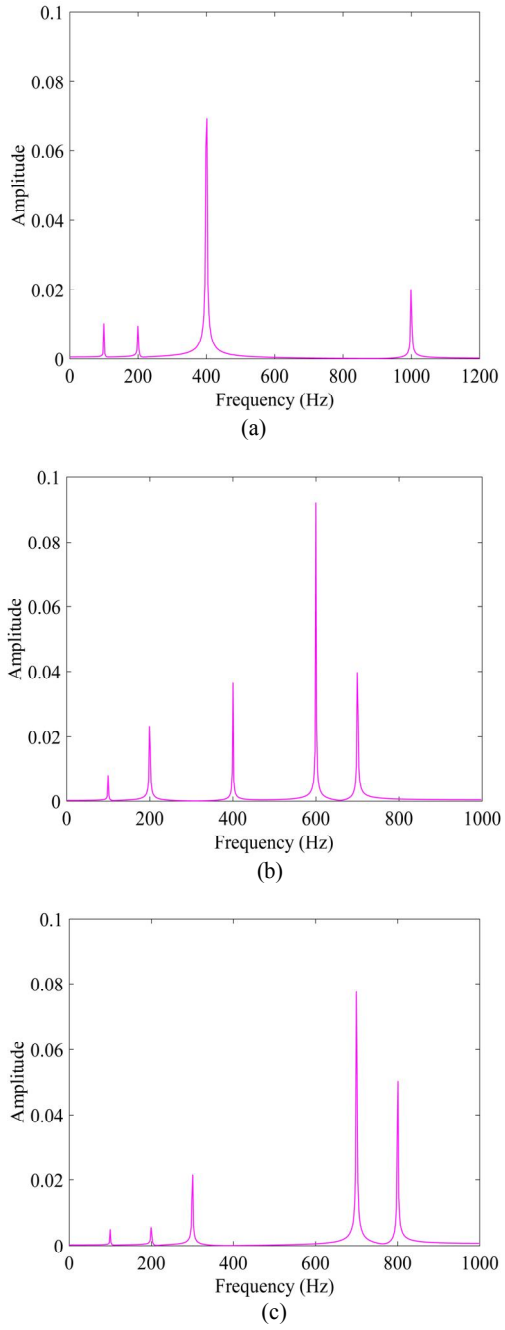

Fig. 16. Hilbert marginal spectrum of three fault conditions: (a) core deformation, (b) winding deformation, (c) winding looseness

by length, only the Hilbert marginal spectrum of sensor tag5 under three different fault conditions are displayed in Fig. 16.

From Fig. 16 it can be seen that the distribution of Hilbert marginal spectrums under these three fault conditions are quite different from that of normal condition. The amplitude of fundamental frequency component (100 Hz) is much smaller than that of normal condition, and these three Hilbert marginal spectrums contain more harmonic components, which are mainly focused within 300-1000 Hz. Table 4-6 reveal the similarities between the three fault conditions and normal condition, respectively.

Table 4 shows the HMS similarities between core deformation and normal condition. According to this table, all the $S_{tag,\ ref}$ are all below 60%, besides, the minimum $S_{tag,\ ref}$ appears between sensor tag5 and normal condition, which indicates that the fault location is close sensor tag 5.

Table 5 reveals the HMS similarities between winding deformation and normal conditions. It can be seen that all the $S_{tag,\ ref}$ are all below 50%, and the minimum similarity also appears between sensor tag5 and normal condition. So, the fault can be easily identified.

Table 6 is the HMS similarities between winding looseness and normal conditions. Obviously, all the $S_{tag,\ ref}$ are all below 50%. Likewise, the $S_{tag,\ ref}$ of sensor tag5 and normal condition is also the minimum value, thus the fault can be effectively identified.

From the results and analyses above, the proposed diagnosis method is proven to be effectively. When the $S_{tag,\ ref} > 90\%$, the detected transformer is considered as healthy, if the $S_{tag,\ ref} < 60\%$, the detected transformer is thought to be abnormal. Furthermore, for $40\% < S_{tag,\ ref} < 60\%$, the fault may be the core deformation, and for $S_{tag,\ ref} < 40\%$, the winding failure (deformation or looseness) may occur. Meanwhile, the location of faults can be confirmed according to the value of $S_{tag,\ ref}$ since the value of $S_{tag,\ ref}$ is closely related to the position of sensor tag and fault.

5. Conclusion

In this paper a nondestructive and low cost approach based on self-powered RFID sensor tag and improved HHT is proposed to diagnose transformer in service. The developed sensor tag operates in ultra-high frequency with functionalities of signal acquisition, data storage and data transmission. Solar panel is employed as power supply for the whole circuitry. Supercapacitor is used in this design to improve the power stability. Moreover, a customized charging circuit is adopted to charge the supercapacitor to 4.8V output voltage. A LDO regulator is adopted to stabilize the output voltage. The whole power management circuit including the solar panel, LDO regulator, supercapacitor and charging circuit can provide stable 2.5V DC output voltage.

In this paper, Hilbert marginal spectrum is adopted to diagnose transformer in service by comparing the similarities between measured Hilbert marginal spectrum and reference spectrum (obtained from healthy transformer). To avoid potential aliasing phenomenon, an improved BREMD method which is optimized by QPSO algorithm is proposed to obtain the IMF functions of the raw vibration signals.

Studies in this paper validate the feasibility of the proposed approach in transformer fault diagnosis. For transformer failure types of core deformation, winding deformation, and winding looseness, the mean values of

similarities of Hilbert marginal spectrum are 46.85, 31.67, and 25.73, respectively. The future study will focus on enhancing the real-time ability of diagnosis and the construction of wireless monitoring network for the whole substation.

Acknowledgements

This work was supported by the National Natural Science Foundation of China under Grant No. 51577046, the State Key Program of National Natural Science Foundation of China under Grant No. 51637004, the national key research and development plan "important scientific instruments and equipment development" Grant No.2016YFF0102200, Equipment research project in advance Grant No.41402040301.

References

[1] Bengtsson, C. "Status and trends in transformer monitoring," *IEEE Transactions on Power Delivery*, vol. 11, no. 3, pp. 1379-1384, 1996.

[2] Wang, M.; Vandermaar, A.J.; Srivastava, K.D. "Review of condition assessment of power transformers in service," *IEEE Electrical Insulation Magazine*, vol. 18, no. 6, pp. 12-25, 2002.

[3] Kogan, V.I.; Fleeman, J.A.; Provanzana, J.H. "Failure analysis of EHV transformers," *IEEE Transactions on Power Delivery*, vol. 3, no. 2, pp. 672-683, 1988.

[4] Palani A, Santhi S, Gopalakrishna S. "Real-Time Techniques to Measure Winding Displacement in Transformers During Short-Circuit Tests," *IEEE Transactions on Power Delivery*, vol. 23, no. 2, pp. 726-732, 2008.

[5] Khan S A, Equbal M D, Islam T. "A comprehensive comparative study of DGA based transformer fault diagnosis using fuzzy logic and ANFIS models," *IEEE Transactions on Dielectrics and Electrical Insulation*, vol. 22, no. 1, pp. 590-596, 2015.

[6] L. Coffeen, J. Mcbride, N. Woldemariam, and J. Benach, "A summary of NEETRAC on-line frequency response analysis (FRA) a new EPRI commercial prototype FRA installation at first energy," *in Proceedings of the EPRI Substation Equipment Maintenance Optimiz. Diagnost. San Antonio*, TX, USA, March 2009.

[7] C. Bartoletti, M. Desiderio, D. D. Carlo, G. Fazio, F. Muzi, G. Sacerdoti, and F. Salvatori, "Vibro-acoustic techniques to diagnose power transformers," *IEEE Trans. Power Del.*, vol. 19, no. 1, pp. 221-229, Jan. 2004.

[8] Z. Berler, A. Golubev, V. Rusov, V. Tsvetkov, and C. Patterson, "Vibro-acoustic method of transformer clamping pressure monitoring," *in Proceedings of IEEE Int. Symp. Elect. Insul.*, 2000, pp. 263-266.

[9] S. Ji, Y. Luo, and Y. Li, "Research on extraction technique of transformer core fundamental frequency vibration based on OLCM," *IEEE Trans. Power Del.*, vol. 21, no. 4, pp. 1981-1988, Oct. 2006.

[10] Hong, K.; Huang, H.; Zhou, J. "Winding Condition Assessment of Power Transformers Based on Vibration Correlation," *IEEE Transactions on Power Delivery*, vol. 30, no.4, pp. 1735-1742, 2015.

[11] García B, Burgos J C, Alonso Á M. "Transformer tank vibration modeling as a method of detecting winding deformations-part I: theoretical foundation," *IEEE Transactions on Power Delivery*, vol. 21, no.1, pp. 157-163, 2006.

[12] Kwon G Y, Lee C K, Lee G S, et al. "Off-line Fault Localization Technique on HVDC Submarine Cable via Time-Frequency Domain Reflectometry," *IEEE Transactions on Power Delivery*, vol. 32, issue 3, pp. 1626-1635, June 2017.

[13] Duan R, Wang F. "Fault Diagnosis of On-Load Tap-Changer in Converter Transformer Based on Time-frequency Vibration Analysis," *IEEE Transactions on Industrial Electronics*, vol. 63, no. 6, pp. 1-11, 2016.

[14] Lu D, Qiao W, Gong X. "Current-based fault detection for wind turbine systems via Hilbert-Huang transform," *in Proceedings of* IEEE Power & Energy Society General Meeting. New York, USA, July 2013.

[15] Gu F C, Chang H C, Kuo C C. "Gas-insulated switchgear PD signal analysis based on Hilbert-Huang transform with fractal parameters enhancement," *IEEE Transactions on Dielectrics & Electrical Insulation*, vol. 20, no.4, pp. 1049-1055, 2013.

[16] Soualhi A, Medjaher K, Zerhouni N. "Bearing Health Monitoring Based on Hilbert-Huang Transform, Support Vector Machine, and Regression," *IEEE Transactions on Instrumentation & Measurement*, vol. 64, no. 1, pp. 52-62, 2014.

[17] Z. Wu and N. E. Huang, "Ensemble empirical mode decomposition: A noise-assisted data analysis method," *Adv. Adapt. Data Anal.*, vol. 1, pp. 1-41, 2009.

[18] Q. Y. He, "Ambient exciting modal parameter identification based on modern time-frequency analysis," Ph.D. dissertation, Dept. Elect. Eng., Chongqing Univ., Chongqing, China, 2009.

[19] Sun J, Xu W, Feng B. "A global search strategy of quantum-behaved particle swarm optimization," *in Proceedings of* 2004 IEEE Conference on Cybernetics and Intelligent Systems. California, USA, April 2014.

[20] Ji, S.; Zhu, L.; Li, Y. "Study on transformer tank vibration characteristics in the field and its application," *Przeglad Elektrotechniczny*, vol. 87, no. 2, pp. 205-211, 2011.

[21] Yoon, J.T.; Youn, B.D.; Park, K.M.; Lee, W.R. "Vibration-based robust health diagnostics for

mechanical failure modes of power transformers," *In proceeding of the IEEE conference on Prognostics and Health Management*, Gaithersburg, USA, October 2013.
[22] Deng F, He Y, Bing L. "Design of an Embedded CMOS Temperature Sensor for Passive RFID Tag Chips," *Sensors*, vol. 15, no. 5, pp. 11442-11450, 2015.
[23] Jauregi I, Solar H, Beriain A. "UHF RFID temperature sensor assisted with body-heat dissipation energy harvesting," *IEEE Sensors Journal*, vol. 17, no. 5, pp. 1471-1478, 2016.
[24] Catarinucci L, Colella R, Tarricone L. "Enhanced UHF RFID Sensor-Tag," *IEEE Microwave & Wireless Components Letters*, vol. 23, no. 1, pp. 49-51, 2013.
[25] Donno D D, Catarinucci L, Tarricone L. "RAMSES: RFID Augmented Module for Smart Environmental Sensing," *IEEE Transactions on Instrumentation & Measurement*, vol. 63, no. 7, pp. 1701-1708, 2014.
[26] M. Magno *et al.*, "Extended wireless monitoring through intelligent hybrid energy supply," *IEEE Trans. Ind. Electron.*, vol. 61, no. 4, pp. 1871-1881, Apr. 2014.
[27] Raghunathan, V.; Kansal, A.; Hsu, J.; Friedman, J.; Srivastava, M.B. "Design considerations for solar energy harvesting wireless embedded systems," *In Processing of IEEE International Symposium on Information in Sensor Networks.* Boise, USA, April 2015.
[28] S. C. Oliveira, E. Fontana, and F. J. M. M. Cavalcanti, "Leakage current activity on glass-type insulators of overhead transmission lines in the northeast region of Brazil," *IEEE Trans. Power Del.*, vol. 24, no. 2, pp. 822-827, Apr. 2009.
[29] Supercapacitor Charger. Available: http://www.linear.com.cn/product/ltc3225
[30] PowerPath Prioritizer. Available: http://www.linear.com.cn/product/LTC4419.
[31] VI Service Network, available: http://www.vi-china.com.cn/html/ywb/list_1163.html.

Tao Wang received the B.S. degree in electrical engineering from Hefei University of Technology, Hefei, China, in 2014. He is now pursuing the Ph.D. degree in electrical engineering from Hefei University of Technology. His current interests include signal processing, and diagnosis and prognosis of high voltage equipment.

Yigang He received the M.Sc. degree in electrical engineering from Hunan University, Changsha, China, in 1992 and the Ph.D. degree in electrical engineering from Xi'an Jiaotong University, Xi'an, 2 China, in 1996. He currently works as the Head of School of Electrical Engineering and Automation, Hefei University of Technology. His teaching and research interests are in the areas of testing and fault diagnosis of analog and mixed-signal circuits, electrical signal detection, smart grid, radio frequency identification technology, and intelligent signal processing. He has published some 200 journal and conference papers in the aforementioned areas and several chapters in edited books.

Tiancheng Shi was born in 1990, and graduated in 2013 with a bachelor degree of engineering in Hefei University of Technology and is a PhD student in Hefei University of Technology now. His present research interests include fault diagnosis and fault tolerance for power electronics converter systems.

Bing Li received the B.E. degree in automobile engineering from Chongqing Science and Technology University, Chongqing, China, in 1995, and the M.E. and Ph.D. degrees in electrical engineering from Hunan University, Changsha, China, in 2006 and 2011, respectively. He is a associate professor in School of Electrical and Automation Engineering, Hefei University, Hefei, China, since 2013. His current research interests include radio frequency identification technology, wireless sensor networks, and signal processing.